Mid-infrared optical parametric generator with extra-wide (3–19-μm) tunability: applications for spectroscopy of two-dimensional electrons in quantum wells

K. L. Vodopyanov

Interactive Radiation, 181 Legrand Avenue, Northvale, New Jersey 07647

Received February 3, 1999

Using a $\lambda = 2.8\ \mu$m pump makes it possible to take full advantage of notable nonlinear optical properties of the infrared crystals $ZnGeP_2$, CdSe, and GaSe to achieve efficient mid-infrared frequency downconversion. Traveling-wave optical parametric generators with angular tuning were pumped by single 100-ps 2.8-μm Er,Cr:YSGG laser pulses. The continuous tuning range achieved was 3.9–10 μm ($ZnGeP_2$), 3.57–4.3 and 8–13 μm (CdSe), and 3.3–19 μm (GaSe), with a quantum conversion efficiency of typically 10% and the lowest, to the author's knowledge, threshold ever obtained for a traveling-wave optical parametric generator. A dual-wavelength optical parametric generator was used for nonlinear spectroscopy of intersubband transitions of conduction-band electrons, quantum confined in semiconductor quantum wells, as well as for the study of intersubband-based resonantly enhanced $\chi^{(2)}$ in quantum wells.
[S0740-3224(99)01909-8]

OCIS codes: 190.0190, 140.5680, 190.2620, 190.4970, 190.4720.

1. INTRODUCTION

Optical parametric oscillators (OPO's) and optical parametric generators (OPG's) are the most attractive coherent sources of continuously tunable radiation. This is especially true for the mid-IR because of the lack of continuously tunable lasers in this spectral region. At the heart of an OPO or an OPG is the nonlinear optical (NLO) crystal, and, as follows from general principles, linear and NLO susceptibilities in crystals dramatically increase as the bandgap of the material decreases. In particular, the NLO figure of merit, corresponding to the second-order nonlinearity in crystals (with broken central symmetry), increases to almost a fifth order of a short-wave transparency cutoff wavelength $\lambda_{\min}$ (which is proportional to the inverse bandgap energy E_g). This is illustrated in Fig. 1, where the NLO figure of merit d^2/n^3 (here $d = d_{\mathrm{NL}}$ is the NLO coefficient, and n is the average refractive index near the center of transparency) of most of the crystals used in nonlinear optics is plotted, on a log–log scale, as a function of the short-wave transparency cutoff wavelength. A substantial portion of the data was taken from the handbook written by Dmitriev *et al.*[1]

In fact, according to Miller's rule,[2] $d_{\mathrm{NL}} \propto \chi(\omega_1)\chi(\omega_2)\chi(\omega_3) \propto \chi^3 \propto (\epsilon - 1)^3 \propto (n^2 - 1)^3$, where χ is the linear susceptibility and ϵ is the dielectric constant. Empirically, $\chi \propto (n^2 - 1) \propto 1/E_g \propto \lambda_{\min}$,[3] which implies (at $n^2 \gg 1$) that $(d_{\mathrm{NL}}^2/n^3) \propto (\lambda_{\min})$.[4,5]

A single-pass power parametric gain (for zero phase mismatch) is $\cosh^2(\Gamma L)$, where Γ, the gain increment, is given by

$$\Gamma^2 = \left(\frac{d_{\mathrm{eff}}^2}{n^3}\right)\frac{2\omega_1\omega_2 I_{\mathrm{pump}}}{\epsilon_0 c^3}. \qquad (1)$$

Here I_{pump} is the pump laser intensity; ω_1 and ω_2 are the idler and signal frequencies, respectively; and d_{eff} is the effective nonlinearity d_{NL}.

Thus, for crystals with the longer-wave transparency range, an increase of $(d_{\mathrm{NL}}^2/n^3) \sim \lambda^5$ will overpower the decrease that is due to the frequency factor $\omega_1\omega_2 \sim 1/\lambda^2$ (we assume that the pump, signal, and idler wavelengths will be proportionally shifted). Hence $\Gamma^2 \sim \lambda^3$, which means that an OPO threshold ($\sim 1/\Gamma^2$) is expected to decrease by approximately an order of magnitude per one octave shift into the IR.

It will be shown in this paper that, with an appropriate pump laser, the IR crystals $ZnGeP_2$ (ZGP), CdSe, and GaSe can be used for efficient frequency downconversion into the mid-IR with unprecedently low pump thresholds and with the largest, to my knowledge, wavelength range of mid-IR tunability (3–19 μm), ever obtained with OPO's or OPG's. Some applications in the field of spectroscopy of condensed matter, with a dual-wavelength OPG, will also be presented.

2. NONLINEAR OPTICAL CRYSTALS

The main features of $ZnGeP_2$, CdSe, and GaSe NLO crystals employed in the present experiments include a wide mid-IR transparency range, a high NLO figure of merit, the capability of being phase matched in a broad spectral interval, and a high laser damage threshold. Owing to recent advancements in crystal growth, it is now possible to grow single crystals with excellent optical quality. Some linear and NLO properties of $ZnGeP_2$, CdSe, and GaSe are listed in Table 1.

A. $ZnGeP_2$

The most prominent feature of ZGP crystal is that it has the highest second-order nonlinearity ($d_{\text{eff}} = 75$ pm/V) of all the commercially available crystals, corresponding to its NLO figure of merit (Table 1), which is 60 times larger than that of $LiNbO_3$. In the 2.6–8.4-μm spectral range ZGP has a linear absorption coefficient α that is below 0.03 cm^{-1}. At $\lambda \approx 2$ μm a typical value of α is near 0.08 cm^{-1} (measured for an ordinary ray). Between 8 and 12 μm the transmission is hampered because of multiphonon absorption.

The unique properties of ZGP favor a variety of NLO applications, including OPO's and OPG's. ZGP was first pioneered as an OPO–OPG material in 1985 with a 2.94-μm pump laser.[4] In a more recent study[5] a ZGP OPO pumped by a 2.8-μm, Er,Cr:YSGG laser yielded a 29% quantum conversion efficiency and a forward idler output of 0.7–2.4 mJ in the wavelength range from 6.9 to 9.9 μm. The signal and idler bandwidths were typically 4 cm^{-1}. Mid-IR OPO's with high average output power have been built with ZGP. The type I OPO with a 14-mm ZGP crystal was pumped at 10 kHz by 11-ns, $\lambda = 2.05$ μm pulses from a Ho,Tm:YLF laser.[6] At the maximum pump drive level of 20.1 W incident upon the OPO crystal, the output average power (signal at 3.67 μm, idler at 4.67 μm) reached 10.1 W, corresponding to a conversion efficiency of 50.2%. In another study[7] the type I ZGP OPO was pumped at 2.13 μm with a KTP OPO, and its output, tunable between 3.7 and 4.8 μm, reached an average power of 22 W. In a coupled tandem OPO (OPO within an OPO design)[8] a type I ZGP OPO was also pumped by a KTP OPO (pumped, in turn, at 1.064 μm). The device had an overall quantum slope efficiency of 35% (and an energy efficiency of 5.2% from 1.06 μm to the long mid-IR) and was tunable between 2.7 and 8 μm. In Ref. 9 a type II ZGP traveling-wave OPG was pumped by an output of a seeded optical parametric amplifier ($\lambda \approx 3$ μm) with a 2.7-ps pulse duration. With a two-pass arrangement (OPG–optical parametric generator) the 5–11-μm tunability was achieved with microjoule output energies and 20% internal quantum efficiency. The traveling-wave OPG threshold was <100 MW/cm^2 for a crystal length of only 1 cm.

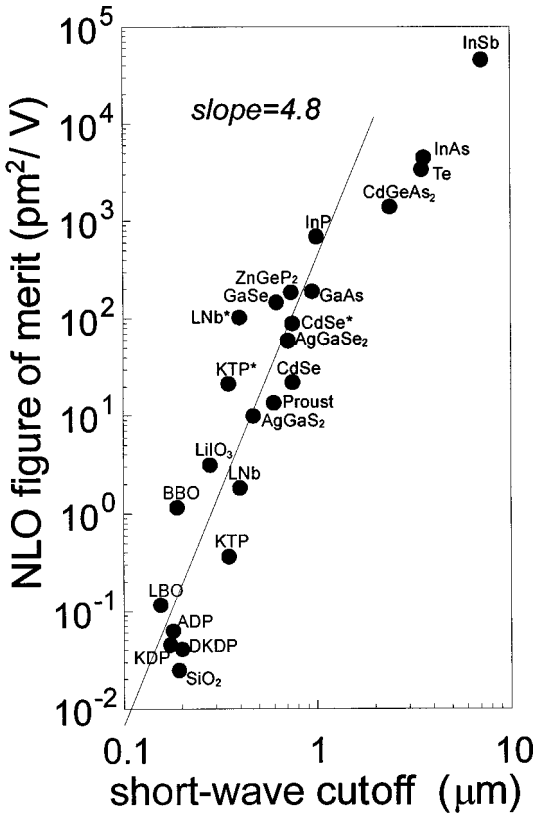

Fig. 1. Figure of merit d^2/n^3 for the most common NLO crystals, plotted as a function of the short-wave transparency cutoff wavelength. In some cases, when there are different tensor components in use (e.g., d_{31} and d_{33} for $LiNbO_3$), two different values are plotted for the same material.

B. CdSe

The CdSe crystal was first explored as a NLO material for OPO's[10,11] and difference-frequency generation[12,13] at the beginning of the seventies. Despite the fact that its NLO coefficient, $d_{31} = 18$ pm/V, is three and four times smaller[1] than that of GaSe and ZGP, respectively, it has certain advantages. CdSe is a binary crystal with a mature growing technology and has a wide transparency range (0.75–25 μm) and extremely low optical losses (<0.01 cm^{-1} over the 1–10-μm region); in addition, long (>5 cm) crystals can be grown routinely.

A CdSe OPO pumped by a 2.8-μm, Er,Cr:YSGG laser produced a 59% signal-plus-idler slope efficiency, exceeding that of ZGP at the same pump conditions. The total idler output was 1.2–2.4 mJ between 8.5 and 12.3 μm (at a linewidth of ~ 4 cm^{-1}), and the idler beam divergence was 2.2–2.5 times the diffraction limit.[5]

C. GaSe

First explored as a NLO material in 1972,[14] GaSe has been successfully used, since then, for second-harmonic generation (SHG) and sum- and difference-frequency generation.[15] GaSe has a number of very positive properties for NLO applications. Foremost among these are its extreme transparency (0.62–20 μm, significantly larger than in ZGP) and its high second-order nonlinear-

Table 1. Some Properties of Mid-IR Nonlinear Crystals[a]

Crystal	Transmission Range (μm)	n_o[b]	n_e[c]	Nonlinearity d_{eff} (10^{-12} m/V)	NLO Figure of Merit d^2/n^3 (10^{-24} m^2/V^2)
ZGP	0.74–12.5	3.13	3.17	75	180
CdSe	0.75–25	2.44	2.46	18	22
GaSe	0.62–20	2.85	2.46	54.4	128

[a] Ref. 1. In column headings, *o* stands for ordinary; *e*, for extraordinary.

ity (d_{NL} = 54.4 pm/V), which is among the top five such nonlinearities measured for birefringent crystals. Owing to its very large birefringence ($\Delta n \sim 0.35$), GaSe can satisfy phase-matching (PM) conditions for most of the three-wave processes within the transparency region. On the negative side, GaSe is a soft, layered material that can be cleaved only along the 001 plane (*z*-cut orientation); it also has a large birefringent walk-off. Whereas one can solve the problem associated with its softness by attaching the crystal to a metal holder, the PM polar angles are generally small (10–20°) because of the large birefringence, and a *z*-cut orientation is suitable in most cases.

As a result of the advancement of the growth technology, GaSe became, in the beginning of the nineties, the focus of a renewed research and development effort: The first OPG was demonstrated with Er:YAG ($\lambda = 2.94\,\mu$m)[16] and Er:Cr:YSGG ($\lambda = 2.8\,\mu$m)[17] laser pumping, and picosecond and subpicosecond pulses of light, with tunability between 4 and 20 μm, were generated by frequency mixing of near-IR pulses in GaSe.[18,19] Recently, mid-IR pulses were generated in GaSe by phase-matched difference-frequency mixing within the broad spectrum of the same 20-fs-long pulse from a mode-locked Ti:sapphire laser.[20] 140-fs pulses, continuously tunable in the wavelength range of 9–18 μm, were demonstrated.

3. LASER SOURCE

The choice of a proper pump laser for an OPO or an OPG is almost as important as the choice of the NLO crystal. It is tempting to choose a commercial laser fitting the crystal's transmission window (e.g., Nd:YAG, with the wavelength close to 1:06 μm); however, there are several limitations, especially with regard to a long-wave OPO:

- The pump laser wavelength should not be too close to the crystal's short-wave transparency cutoff. Proper choice of the pump laser wavelength will help to avoid linear absorption associated with impurity centers with energy levels inside the bandgap;
- If the pump wavelength is too short as compared with the OPO output, then the OPO energy conversion efficiency might be quite low because of the photon energy differences (quantum defect). For example, if the OPO quantum conversion efficiency is 50%, the pump wavelength is at 1.06 μm, and the OPO output is at 10 μm, then the energy (or power) conversion will be only 5%;
- When the pump laser photon energy is larger than half the NLO crystal's bandgap, two-photon absorption (TPA) may become a severe limitation of the OPO performance (both TPA and parametric gain are intensity dependent and give contributions of the opposite sign). For example, in our previous work,[21] the TPA coefficient was measured in GaSe at $\lambda \approx 0.7\,\mu$m (corresponding to $E_g/2 < \hbar\omega < E_g$) to be $\beta = 6 \times 10^{-9}$ cm/W. This implies that even at 20 MW/cm^2 a noticeable TPA will occur (12% at L = 1 cm).

Thus, ideally, the pump laser wavelength should be somewhere close to the center of the spectral transmission curve of the NLO crystal.

As a pumping laser source an Er,Cr:YSGG laser with $\lambda \approx 2.8\,\mu$m (2.797 μm) was chosen. There are at least four reasons for this choice: (i) 2.8 μm is sufficiently far from the short-wave transparency cutoff of crystals like ZGP, GaSe, and CdSe; thus absorption at this wavelength can be made small ($\alpha \sim 0.01\,\text{cm}^{-1}$); (ii) the quantum defect, determined by the difference between the pump and the OPO output photon energies, is small because of the sufficiently long-wave pump; (iii) there is an absence of TPA at the pump wavelength [for the same reason as in (ii)]; and, finally (iv) an Er,Cr:YSGG laser has high efficiency and robustness.

4. TRAVELING-WAVE OPTICAL PARAMETRIC GENERATOR

A traveling-wave (mirrorless) superfluorescent OPG scheme was favored in the present experiment so that the results might benefit from the extremely large nonlinear figure of merit of the mid-IR crystals ZGP, GaSe, and CdSe. The principle of operation is based on the high-gain ($>10^{10}$) amplification of quantum noise in a nonlinear crystal pumped by intense short laser pulses in a double-pass configuration. The traveling-wave configuration makes it possible to have the OPG output in the form of a single intense pulse.

The main advantages of the traveling-wave OPG scheme are

- Simplicity of the optical design (no cavity);
- Ability to produce very high peak power outputs (>1 MW) in a single short pulse;
- Broad tunability (over the crystal's transparency range), restricted only by PM conditions;
- No buildup time—hence the possibility of generating two or more synchronized, independently tunable pulses from different OPG's pumped by the same laser (attractive for laser spectroscopy).

A schematic diagram of the OPG is presented in Fig. 2. Single 100-ps pulses of an actively mode-locked, *Q*-switched, cavity-dumped Er,Cr:YSGG laser (TEM_{00} mode; beam diameter, ~1 mm)[22] are amplified in a four-pass amplifier to yield an energy of ~3 mJ at a repetition rate of 3 Hz. A two-pass OPG setup uses a dichroic beam-splitting mirror (highly reflective at the laser wavelength and highly transmissive at the OPG wavelengths) and a back-reflecting gold mirror. A lens *L* was used to

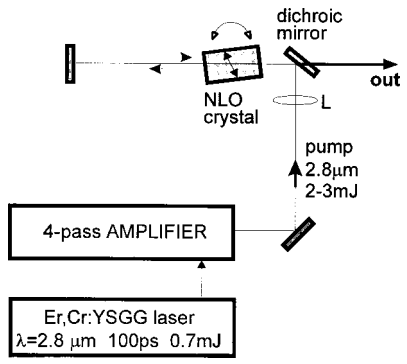

Fig. 2. Schematic of the double-pass traveling-wave OPG pumped by an Er laser.

slightly focus the laser beam into the crystal in such a manner that the laser intensity at the second pass through the crystal was three to four times higher than at the first pass, owing to stronger focusing, and amounted to a few gigawatts per square centimeter. Thus the first pass serves as a superluminescent seed; the second, as a parametric amplifier. This focusing is done to ensure that the parametric gain reaches saturation at the second pass, thus giving maximum conversion efficiency.

Compared with a single-pass geometry, the double-pass OPG scheme produces much smaller (almost diffraction-limited) output beam divergence. Therefore the output OPG beam can be focused to a much tighter (~10λ-diameter) spot, allowing beam intensities of as high as 10^9 W/cm^2 to be created.[23] In the same manner, the OPG output spectral width in a two-pass scheme was reduced owing to the restraint of noncollinear interactions.

5. OPTICAL PARAMETRIC GENERATOR EXPERIMENTAL RESULTS

Figure 3 shows experimental tuning curves (along with the measured crystals' linear transmission) for ZGP, CdSe, and GaSe, obtained in a two-pass OPG scheme for the type I and type II PM and the $\lambda = 2.8\,\mu$m pump. The output OPG radiation was registered with a 25-cm grating monochromator and a mercury cadmium telluride detector or pyrodetector. The vertical bars in Fig. 3(a) correspond to experimental half-maximum linewidths. An excellent fit of the experimental tuning curves to the theoretical ones, calculated on the basis of known dispersion relations, was obtained. The solid curves are based on calculations with the best sets of dispersion relations for ZGP,[24] CdSe,[25] and GaSe,[26] correspondingly.

The type I OPG linewidth (ZGP and GaSe) strongly depends on the wavelength: It is very large (>100 cm^{-1}) near the degeneracy point and decreases as the signal and the idler waves diverge. The type II linewidth is narrower (~10 cm^{-1}, Fig. 4) and is less dependent on the wavelength, in agreement with the calculated acceptance bandwidth.[27]

Figure 5 represents the OPG's quantum conversion efficiency as a function of the wavelength, and Table 2 summarizes results obtained with ZGP, CdSe, and GaSe. The quantum conversion efficiency in a two-pass OPG was 5–10% at an I_{pump} of ~3–5 GW/cm^2 for all three crystals [in a single-pass scheme it can be higher—17.6% (ZGP)—at the expense of the beam quality]. Uncoated crystals were used, with Fresnel reflections creating substantial losses; thus conversion efficiency can be improved by at least a factor of 2 with an antireflective coating.

A ZGP OPG has smaller tunability than a GaSe OPG, but its main advantage is a much lower pumping threshold, 90 MW/cm^2 ($L = 4$ cm), owing to higher nonlinearity.

As far as the CdSe crystal is concerned, its tuning range has a gap because only type II PM is possible. Yet, in the important spectral range of 8–12 μm, the CdSe OPG is superior (in the sense of efficiency and linewidth) to ZGP and GaSe.[28]

Continuous tunability from 3.3 to 19 μm (covering almost 3 octaves) has been achieved with a single GaSe crystal. This is, to my knowledge, the largest wavelength range of tunability ever obtained with an OPG or an OPO. A cylindrical focusing of the pump beam at the second pass, with an aspect ratio of 1:10–1:20, was used (Fig. 2) because of GaSe's huge walk-off (0.8 mm for a crystal with $L = 1.4$ cm and a PM angle $\theta \approx 12°$), to keep

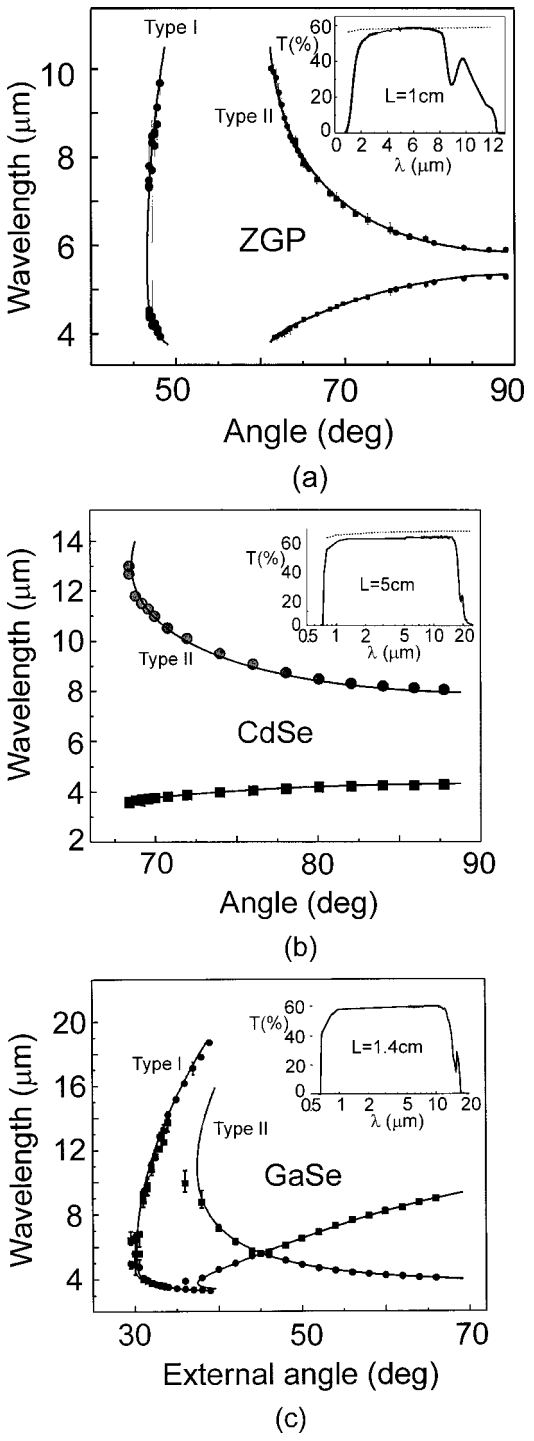

Fig. 3. OPG angular tuning curves at a $\lambda = 2.8\,\mu$m pump for (a) ZGP, (b) CdSe, and (c) GaSe (z cut). Vertical bars [in (a)] represent experimental half-maximum linewidths. Solid curves represent calculated tuning curves based on best dispersion relations for ZGP,[24] CdSe,[25] and GaSe,[26] accordingly. Insets: linear transmission spectra for uncoated crystals; dotted lines correspond to Fresnel losses.

the beam size sufficiently large in the kz plane (k is the wave vector; z is the optical axis). The OPG threshold was high enough (1.1 GW/cm^2), primarily because of the crystal's small length (1.4 cm).

The OPG pulse duration was measured by an autocorrelation technique to be 75–90 ps, with a 2-mm GaSe crystal being used as a noncollinear second-harmonic generator. A shortening of the OPG pulse duration, compared with that of the pump laser, is apparently due to the nonlinearity of the frequency conversion process.

Thus light tunable between 3.3 and 19 μm can be generated in an OPG with short pulses of $\lambda = 2.8\,\mu$m radiation, with ZGP exhibiting the best performance in the spectral range of 4–8 μm; CdSe, between 8 and 12 μm; and GaSe, beyond 12 μm.

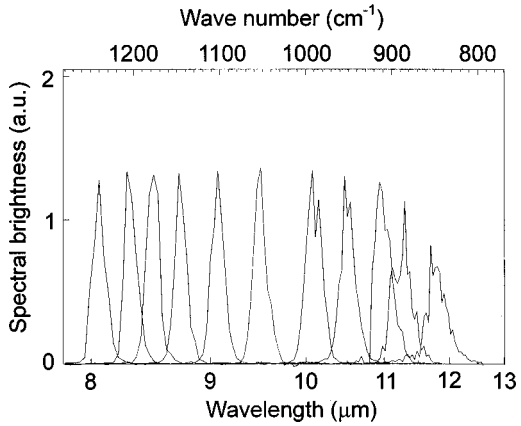

Fig. 4. CdSe OPG line shapes at different wavelengths, corresponding to angle tuning.

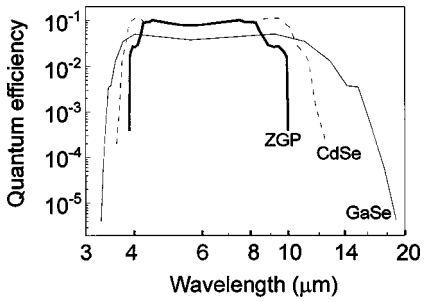

Fig. 5. OPG quantum efficiency as a function of wavelength for the three crystals.

6. APPLICATIONS

Since a traveling-wave OPG does not have buildup time, it is possible to generate two or more independently tunable and perfectly synchronized light pulses from different OPG's, pumped by the same laser, as illustrated in Fig. 6. Therefore such an OPG can be a convenient source for two-color solid-state spectroscopy.

When a thin (~10-nm) layer of one semiconductor (e.g., GaInAs) is sandwiched between two layers of another semiconductor, with a larger bandgap (e.g., AlInAs), carriers are trapped in two dimensions, owing to the potential barrier. This sandwich structure, repeated many times, is called a multiple quantum well (MQW). As a result of quantum confinement in the direction perpendicular to the layers, discrete energy states (or subbands) occur [Fig. 7(a) below], in both the conduction and the valence bands, which dramatically change the electronic, magnetic, and optical properties of the material. Corresponding transitions [intersubband (ISB) transitions] lie in the mid- or far-IR region of the spectrum; they have narrow linewidths and extremely large transition dipole moments, which makes them attractive for a variety of applications (see, e.g., Ref. 29). The present research is focused on spectroscopic studies of the dynamics of ISB transitions and novel NLO properties associated with these resonances.

A. Two-Color Spectroscopy of Intersubband Transitions in a Multiple Quantum Well

Carrier distribution between and within subbands of a semiconductor MQW system under strong electrical or optical excitation is of great interest from two viewpoints: the underlying physics, and device fabrication. In this study two-color ISB pump–probe spectroscopy was used in a three-level InGaAs/InAlAs quantum-well system to examine the electron distribution under intense ($I \gg I_{sat}$) quasi-stationary [from ($n = 1$) to ($n = 2$)] excitation.

MQW samples consist of forty 10-nm-thick n-doped InGaAs wells, separated by 10-nm undoped InAlAs barriers.[30] The relevant ISB transitions energies are $E_{12} = 139$ meV ($\lambda = 8.9\,\mu$m) and $E_{23} = 172$ meV (7.2 μm). A double-pass 45° waveguide geometry was used to couple p-polarized light to ISB transitions.[31] Experiments were performed at $T = 30$ K so that only the lower ($n = 1$) state was populated [hence transition ($n = 2$) to

Table 2. Experimental Results Obtained with the ZGP, CdSe, and GaSe Two-Pass OPG's Pumped at $\lambda = 2.8\,\mu$m

Crystal	Tuning Range (μm)	Typical Linewidth (cm^{-1})	OPG Pump Threshold (GW/cm^2)	Quantum Conversion Efficiency (%)
ZGP	3.9–10 (type I)	100	0.5 ($L = 1.1$ cm)	10
	3.9–5.3, 5.8–10 (type II)	10	0.09 ($L = 4$ cm)	
CdSe	3.6–4.3, 8–13 (type II)	10	0.47 ($L = 5$ cm)	10
GaSe	3.3–19 (type I)	10–50	1.1 ($L = 1.4$ cm)	5
	3.9–10 (type II)	20–30		

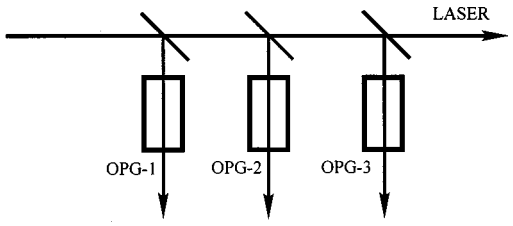

Fig. 6. Multicolor OPG setup pumped by the same laser pulse.

($n = 3$) was not seen at normal conditions]. Figure 7(a) shows MQW subbands (corresponding to the electron motion perpendicular to the layers) and energy dispersion in the plane, parallel to the layers. Figure 7(b) depicts linear MQW absorption spectrum, obtained with an attenuated OPG beam.

In the present pump and probe experiments two independently tunable beams from a dual-beam OPG[32] were focused onto the sample (both had a pulse duration of ~80 ps). The maximum pump intensity (in a 300-μm spot) was 20 MW/cm^2. A much weaker probe beam (at zero time delay) was frequency tuned (within the range of 6–12 μm), thus monitoring transmission changes induced by the pump.

Because of nonparabolicity, different subbands have different effective masses (for instance, $n = 2$ mass is heavier than $n = 1$ mass): ISB transitions corresponding to higher-lying states at larger k_{II} values are redshifted [Fig. 7(a)] as compared with those in the Brillouin-zone center. Thus one can map the in-plane electron energy distribution by probing absorption at different frequencies.

Figure 7(b) shows the ISB spectrum in the presence of a strong saturating pump, resonant to the ($n = 1$) to ($n = 2$) transition ($\lambda \approx 9\ \mu$m), with intensity $I = 20$ MW/cm^2, which is ~100 times the saturation intensity. The following features were observed:

- The ($n = 1$) to ($n = 2$) transition line was almost completely bleached;
- No spectral hole was seen at the pump frequency, which indicates the advantage of predominantly homogeneous broadening of the ISB transition;
- Induced absorption from ($n = 2$) to ($n = 3$) appears on the blue side of the 1–2 resonance peak [the result of populating the ($n = 2$) subband];
- The two peaks of the induced absorption are clearly seen on the red side. It is believed that these correspond to the excess carrier occupancy of the high-lying states in the ($n = 1$) electron subband, which is associated with the 2–1 ISB scattering path created by LO emission or absorption [Fig. 7(a)]. It is well established that ($n = 2$) electrons scatter (with a lifetime of typically 1 ps) to the ($n = 1$) subband, by phonon emission or absorption, and create excess population in high-lying states of the lower ($n = 1$) subband. The two arrows in the inset of Fig. 7(b) indicate the calculated position of the peaks (InGaAs LO phonon energy $\hbar\omega_{LO} = 34$ meV; effective mass, $0.043m_0$; and nonparabolicity data from Ref. 30).

At $T = 30$ K the LO phonon occupancy n_{ph} tends to zero as $kT \ll \hbar\omega_{LO}$, and one should observe only phonon emission. However, at the condition of strong laser excitation the hot phonon occupancy can be well above unity [each electron scattered from ($n = 2$) to ($n = 1$) creates roughly 139 meV/34 meV = 4 phonons, and the phonon lifetime is comparatively long: ~5 ps]. Therefore phonon emission ($\propto n_{ph}$) and absorption [$\propto(n_{ph} + 1)$] processes may be quite comparable.

Thus a strongly nonthermal electron distribution in a MQW system subjected to saturating ($n = 1$) to ($n = 2$) excitation was observed. Two humps in the distribution of carriers in k space [the ($n = 1$) subband] occur because of the electrons, which are backscattered from ($n = 2$) to ($n = 1$) by phonon emission or absorption.

B. Second-Harmonic Generation in Multiple Quantum Wells

Specially engineered asymmetric quantum wells possess resonant second- and third-order optical nonlinearities that are three and five orders of magnitude, respectively, higher than that in the bulk semiconductors (GaAs),

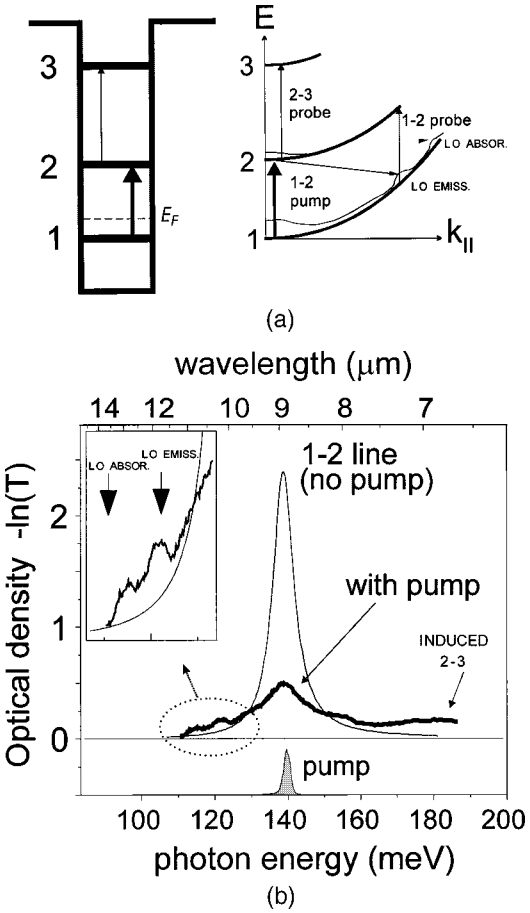

Fig. 7. (a) Conduction-band energy subbands in MQW's and energy dispersion in the plane, parallel to the layers. Electrons, scattered from the ($n = 2$) to the ($n = 1$) subband by phonon emission or absorption, create excess population in high-lying states of the lower ($n = 1$) subband. (b) Linear MQW [from ($n = 2$) to ($n = 1$)] absorption spectrum (thin curve), and the spectrum obtained when the saturating pump is applied (thick curve). Induced absorption from ($n = 2$) to ($n = 3$) can be seen on the blue side. The two peaks on the red side correspond to excess carrier occupancy in high-lying states of the ($n = 1$) subband, a condition that is due to electrons backscattered by phonon emission or absorption. The two arrows in the inset indicate theoretical positions of the peaks.

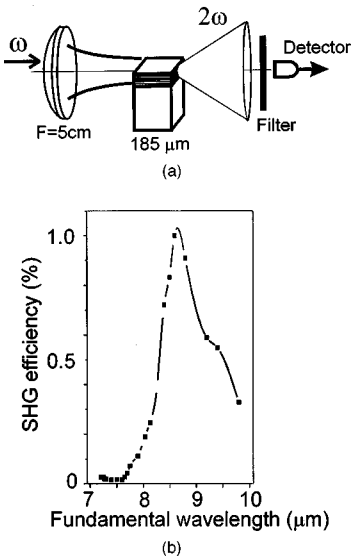

Fig. 8. (a) Schematic of the experiment on SHG in asymmetric MQW's, performed with edge-emitting geometry; (b) SHG efficiency versus incident wavelength. The pump intensity is ~50 MW/cm^2.

which may be used for frequency mixing, phase conjugation, and all-optical modulation.[33–36]

An asymmetric double-quantum-well structure specially designed for SHG was grown at Sheffield University (Sheffield, UK) by molecular beam epitaxy and consisted of an active SHG region placed between the two PM regions.[37] The active region incorporates 178 periods of repeated asymmetric InGaAs/InAlAs double quantum wells (27-Å $In_{0.53}Ga_{0.47}As$ well/18-Å $In_{0.52}Al_{0.48}As$ barrier/ 49-Å $In_{0.53}Ga_{0.47}As$ well/100-Å $In_{0.52}Al_{0.48}As$ barrier) with subband resonances close to the $\lambda = 8-9\ \mu m$ pump wavelength and its second harmonic. The PM region consists of 139 periods of a MQW (58-Å $In_{0.53}Ga_{0.47}As$ well/100-Å $In_{0.52}Al_{0.48}As$ barrier). Thus, the net epilayer thickness (PM plus active layer) was $\approx 8\ \mu m$.

Two geometries were used: (i) edge-emitting waveguide geometry, in which the light propagated along the MQW layers [Fig. 8(a)] and the PM (which, despite the sample's short length, 185 μm, was essential inasmuch as the coherence length was only 40 μm) was achieved by the presence of the PM region, which modifies (by the Kramers–Kronig relation) the dispersion of light in the desired way; and (ii) 45° wedge multibounce geometry, in which the phases of second-harmonic waves generated at sequential bounces were synchronized by means of a change of the angle of incidence.[37] As a light source an idler beam of an Er-laser-pumped ZGP OPG, which was tunable within the range $\lambda = 7-10\ \mu m$, was employed. Single OPG pulses with energies of a few microjoules and 90-ps pulse duration were focused onto the sample [Fig. 8(a)] by a 5-cm BaF_2 lens so that the spot size was ~100 μm, with a peak radiation intensity of up to 10^8 W/cm^2.

Figure 8(b) shows the SHG efficiency change observed as the OPG wavelength was tuned. Unlike in bulk materials, the $\chi^{(2)}$ value in MQW's is based on resonantly enhanced ISB nonlinearity and, thus, is frequency dependent. The maximum conversion efficiency was observed at $\lambda = 8.6\ \mu m$, which is amazingly close to that expected from the design—8.5 μm.

Optical SHG, with a record (for ISB-based devices) efficiency of ~1% and a resonance peak near the fundamental wavelength of 8.6 μm, was achieved with an asymmetric MQW structure with manmade ISB-based dispersive and NLO properties. The length of the sample was only 185 μm. Thus gigantic ISB-based optical nonlinearities in MQW's may be very favorable for creating integrated $\chi^{(2)}$ and $\chi^{(3)}$ devices.

7. CONCLUSION

This study demonstrates that short 2.8-μm erbium-laser pulses can be successfully used for pumping traveling-wave optical parametric generators to generate mid-IR coherent radiation with an extrawide tunability, up to 3–19 μm, with megawatt peak power and a quantum conversion efficiency of ~10%. Such an optical parametric generator was used for the spectroscopic study of two-dimensional electrons confined in semiconductor quantum wells and for the second-harmonic generation of mid-IR light, by means of gigantic $\chi^{(2)}$, resonantly enhanced near MQW intersubband transition frequencies.

ACKNOWLEDGMENTS

The author is grateful to C. C. Phillips for his enthusiasm and support of this work; to G. B. Serapiglia, K. O'Neill, and V. Chazapis for their help in performing experiments; to V. G. Voevodin for manufacturing the high-quality ZGP and GaSe crystals; and to L. A. Kulevskii for valuable discussions. He is also grateful to Carlo Sirtori and Jerome Faist for enlightening discussions and for providing MQW samples; to Geoff Hill and Mark Hopkinson, for SHG MQW sample growth and processing; and to Jerry Meyer and Igor Vurgaftman, for theoretical calculations and design of the SHG MQW structure. This work was supported by the UK Engineering and Physical Sciences Research Council.

The author can be reached by telephone at 201-767-1910, by fax at 201-767-9644, or by e-mail at kvodopyanov@inrad.com.

REFERENCES

1. V. G. Dmitriev, G. G. Gurzadyan, and D. N. Nikogosyan, *Handbook of Nonlinear Optical Crystals* (Springer, Berlin, 1997), pp. 68–240.
2. A. Yariv, *Quantum Electronics* (Wiley, New York, 1988), pp. 378–406.
3. For narrow-gap semiconductors, however, the dependence of the index of refraction on the energy gap becomes weaker: $n^4 E_g = \text{const}$. (Moss rule); see T. S. Moss, *Optical Properties of Semiconductors* (Butterworth, London, 1959), p. 48.
4. K. L. Vodopyanov, V. G. Voevodin, A. I. Gribenyukov, and L. A. Kulevskii, "Picosecond parametric superluminescence in the $ZnGeP_2$ crystal," Bull. Acad. Sci. USSR Phys. Ser. **49**, 146–149 (1985).
5. T. H. Allik, S. Chandra, D. M. Rines, P. G. Schunemann, J. A. Hutchinson, and R. Utano, "Tunable 7–12-μm optical parametric oscillator using a Cr,Er:YSGG laser to pump CdSe and $ZnGeP_2$ crystals," Opt. Lett. **22**, 597–599 (1997).
6. P. A. Budni, L. A. Pomeranz, M. L. Lemons, P. G. Schunemann, T. M. Pollak, and E. P. Chicklis, "10W mid-IR hol-

mium pumped $ZnGeP_2$ OPO," in *Advanced Solid-State Lasers*, W. R. Bosenberg and M. M. Fejer, eds., Vol. 19 of OSA Trends in Optics and Photonics Series (Optical Society of America, Washington, D.C., 1998), pp. 90–92.
7. E. Cheung, S. Palese, H. Injeyan, C. Hoefer, R. Hilyard, H. Komine, J. Berg, and W. Bosenberg, "High power conversion to mid-IR using KTP and ZGP OPO," in *Advanced Solid-State Lasers*, M. M. Fejer, H. Injeyan, and U. Keller, eds., Vol. 26 of OSA Trends in Optics and Photonics Series, (Optical Society of America, Washington, D.C., 1999), pp. 358–361.
8. P. B. Phua, K. S. Lai, R. F. Wu, and T. C. Chong, "Coupled tandem optical parametric oscillator (OPO): an OPO within an OPO," Opt. Lett. **23**, 1262–1264 (1998).
9. V. Petrov, Y. Tanaka, and T. Suzuki, "Parametric generation of 1-ps pulses between 5 and 11 μm with a $ZnGeP_2$ crystal," IEEE J. Quantum Electron. **33**, 1749–1755 (1997).
10. R. L. Herbst and R. L. Byer, "Singly resonant CdSe infrared parametric oscillator," Appl. Phys. Lett. **21**, 189–191 (1972).
11. A. A. Davydov, L. A. Kulevsky, A. M. Prokhorov, A. D. Savel'ev, V. V. Smirnov, and A. A. Shirkov, "A tunable infrared parametric oscillator in CdSe crystal," Opt. Commun. **9**, 234–236 (1973).
12. G. C. Bhar, D. C. Hanna, B. Luther-Davies, and R. C. Smith, "Tunable down-conversion from an optical parametric oscillator," Opt. Commun. **6**, 323–326 (1972).
13. D. C. Hanna, B. Luther-Davies, R. C. Smith, and R. Wyatt, "CdSe down-converter tuned from 9.5 to 24 μm," Appl. Phys. Lett. **25**, 142–144 (1974).
14. G. B. Abdullaev, L. A. Kulevskii, A. M. Prokhorov, A. D. Savel'ev, E. Yu. Salaev, and V. V. Smirnov, "GaSe, a new effective crystal for nonlinear optics," JETP Lett. **16**, 90–92 (1972).
15. N. C. Fernelius, "Properties of gallium selenide single crystal," Prog. Cryst. Growth Charact. **24**, 275–352 (1994).
16. K. L. Vodopyanov, L. A. Kulevskii, V. G. Voevodin, A. I. Gribenyukov, K. R. Allakhverdiev, and T. A. Kerimov, "High efficiency middle IR parametric superradiance in $ZnGeP_2$ and GaSe crystals pumped by an erbium laser," Opt. Commun. **83**, 322–326 (1991).
17. K. L. Vodopyanov and V. G. Voevodin, "2.8-μm laser-pumped type-I and type-II traveling-wave optical parametric generator in GaSe," Opt. Commun. **114**, 333–335 (1995).
18. T. Dahinten, U. Plödereder, A. Seilmeier, K. L. Vodopyanov, K. R. Allakhverdiev, and Z. A. Ibragimov, "Infrared pulses of 1-picosecond duration tunable between 4-μm and 18-μm," IEEE J. Quantum Electron. **29**, 2245–2250 (1993).
19. I. M. Bayanov, R. Danielius, P. Heinz, and A. Seilmeier, "Intense subpicosecond pulses tunable between 4 μm and 20 μm generated by an all-solid-state laser system," Opt. Commun. **113**, 99–104 (1994).
20. R. A. Kaindl, D. C. Smith, M. Joschko, M. P. Hasselbeck, M. Woerner, and T. Elsaesser, "Femtosecond infrared pulses tunable from 9 to 18 μm at an 88-MHz repetition rate," Opt. Lett. **23**, 861–863 (1998).
21. K. L. Vodopyanov, S. B. Mirov, V. G. Voevodin, and P. G. Schunemann, "Two-photon absorption in GaSe and $CdGeAs_2$," Opt. Commun. **155**, 47–50 (1998).
22. K. L. Vodopyanov, "Parametric generation of tunable infrared radiation in $ZnGeP_2$ and GaSe pumped at 3 μm," J. Opt. Soc. Am. B **10**, 1723–1729 (1993).
23. K. L. Vodopyanov and V. G. Voevodin, "Parametric generation of tunable infrared radiation in $ZnGeP_2$ and GaSe pumped at 3 μm," Opt. Commun. **117**, 277–282 (1995).
24. K. Kato, "Second-harmonic and sum-frequency generation in $ZnGeP_2$," Appl. Opt. **36**, 2506–2510 (1997).
25. G. C. Bhar, "Refractive index interpolation in phase-matching," Appl. Opt. **15**, 305–307 (1976).
26. K. L. Vodopyanov and L. A. Kulevskii, "New dispersion relations for GaSe in the 0.65–18 μm spectral region," Opt. Commun. **118**, 375–378 (1995).
27. K. L. Vodopyanov and V. Chazapis, "Extra-wide tuning range optical parametric generator," Opt. Commun. **135**, 98–102 (1997).
28. K. L. Vodopyanov, "Megawatt peak power 8–13 μm CdSe optical parametric generator pumped at 2.8 μm," Opt. Commun. **150**, 210–212 (1998).
29. J. Faist, F. Capasso, D. L. Sivco, C. Sirtori, A. L. Hutchinson, and A. Y. Cho, "Quantum cascade laser," Science **264**, 553–556 (1994).
30. J. Faist, F. Capasso, C. Sirtori, D. L. Sivco, A. L. Hutchinson, S. N. G. Chu, and A. Y. Cho, "Measurement of the intersubband scattering rate in semiconductor quantum wells by excited state differential absorption spectroscopy," Appl. Phys. Lett. **63**, 1354–1356 (1993).
31. K. L. Vodopyanov, V. Chazapis, C. C. Phillips, B. Sung, and J. S. Harris, Jr., "Saturation study of III–V multi-quantum well bound-to-bound and bound-to-quasibound intersubband transitions in the $\lambda = 3–10\ \mu$m spectral range," Semicond. Sci. Technol. **12**, 708–714 (1997).
32. K. L. Vodopyanov, V. Chazapis, and C. C. Phillips, "Two-colour mid-infrared saturation spectroscopy of intersubband transitions in multi-quantum wells," Appl. Phys. Lett. **69**, 3405–3407 (1996).
33. M. M. Fejer, S. J. B. Yoo, R. L. Byer, A. Harwit, and J. S. Harris, Jr., "Observation of extremely large quadratic susceptibility at 9.6–10.8 μm in electric-field-biased AlGaAs quantum wells," Phys. Rev. Lett. **62**, 1041–1044 (1989).
34. E. Rosencher, P. Bols, J. Nagle, and S. Delaitre, "Second harmonic generation by intersub-band transitions in compositionally asymmetric MQWs," Electron Lett. **25**, 1063–1064 (1989).
35. P. Boucaud, F. H. Julien, D. D. Yang, and J.-M. Lourtioz, "Detailed analysis of second-harmonic generation near 10.6 μm in GaAs/AlGaAs asymmetric quantum wells," Appl. Phys. Lett. **57**, 215–217 (1990).
36. G. Almogy and A. Yariv, "Resonantly-enhanced nonlinear optics of intersubband transitions," J. Nonlinear Opt. Phys. Mater. **4**, 401–458 (1995).
37. K. L. Vodopyanov, K. O'Neill, G. B. Serapiglia, C. C. Phillips, M. Hopkinson, I. Vurgaftman, and J. R. Meyer, "Phase-matched second harmonic generation in asymmetric double-quantum wells," Appl. Phys. Lett. **72**, 2654–2656 (1998).